AIChE

Particle Scale Study of Heat Transfer in Packed and Bubbling Fluidized Beds

Z. Y. Zhou and A. B. Yu
Lab for Simulation and Modeling of Particulate Systems, School of Materials Science and Engineering, The University of New South Wales, Sydney, NSW 2052, Australia

P. Zulli
BlueScope Steel Research, P.O. Box 202, Port Kembla, NSW 2505, Australia

DOI 10.1002/aic.11823
Published online March 11, 2009 in Wiley InterScience (www.interscience.wiley.com).

The approach of combined discrete particle simulation (DPS) and computational fluid dynamics (CFD), which has been increasingly applied to the modeling of particle-fluid flow, is extended to study particle-particle and particle-fluid heat transfer in packed and bubbling fluidized beds at an individual particle scale. The development of this model is described first, involving three heat transfer mechanisms: fluid-particle convection, particle-particle conduction and particle radiation. The model is then validated by comparing the predicted results with those measured in the literature in terms of bed effective thermal conductivity and individual particle heat transfer characteristics. The contribution of each of the three heat transfer mechanisms is quantified and analyzed. The results confirm that under certain conditions, individual particle heat transfer coefficient (HTC) can be constant in a fluidized bed, independent of gas superficial velocities. However, the relationship between HTC and gas superficial velocity varies with flow conditions and material properties such as thermal conductivities. The effectiveness and possible limitation of the hot sphere approach recently used in the experimental studies of heat transfer in fluidized beds are discussed. The results show that the proposed model offers an effective method to elucidate the mechanisms governing the heat transfer in packed and bubbling fluidized beds at a particle scale. The need for further development in this area is also discussed. © 2009 American Institute of Chemical Engineers *AIChE J,* 55: 868–884, 2009

Keywords: discrete particle simulation, computational fluid dynamics, heat transfer, heat transfer coefficient, packed beds, fluidized beds

Introduction

Packed and fluidized beds are widely used in industries. Typical examples are ironmaking blast furnace, which involves complicated multiphase flow, heat transfer and chemical reactions in a packed bed,[1,2] and fluidized-bed combustors whose performance heavily depends on the hydrodynamics and thermal-chemical behavior of particles in interaction with gas.[3,4] To achieve optimal design and control of such a fluid-bed reactor, it is important to understand the flow and heat transfer characteristics. Over the past decades, many studies have been carried out in this field, and many empirical correlations have been formulated to determine the heat transfer coefficient (HTC) as, respectively, reviewed by various investigations.[5–8] Those studies are mainly macroscopic, focused on the overall heat transfer behavior. As a result, the resulting correlations are often of limited applicability.

Correspondence concerning this article should be addressed to A. B. Yu at a.yu@unsw.edu.au.

In recent years, heat transfer behavior in a fluidized bed at a microscopic, individual particle level has been examined experimentally.[9–14] In such a study, a hot sphere is immersed in the bed, and its transient temperature is measured using an attached thermocouple. Based on the measured temperature, the HTC can be determined. Such particle scale studies are useful but have limitations in exploring the fundamentals. For example, the heat transfer to a particle should be described by at least three mechanisms, e.g., convection from fluid, conduction from particles or wall, and radiation. However, the contribution of each of these mechanisms is difficult to quantify. Moreover, the heat transfer of a particle will be strongly affected by the local gas-solid flow structure and hence, varies spatially and temporally. The information derived for a single particle may not be reliable because of the difficulty in quantifying the structural information.

Alternatively, mathematical modeling has been increasingly accepted as an effective method to study the heat transfer phenomena in particle-fluid systems. In fact, mechanistic approach based on the packet model originally proposed by Mickley and Fairbanks[15] is a typical one to study the heat transfer between bubbling beds and immersed objects. However, the problem associated with such early approaches is the lack of reliable estimation of parameters.[16,17] This difficulty can be overcome by the newly developed discrete approach. Recently, this approach, mainly based on the so-called discrete particle simulation (DPS), coupled with computational fluid dynamics (CFD), has been widely used in the study of particle-fluid flow, as reviewed recently by Zhu et al.[18] With this DPS-CFD approach, information such as particle-particle or particle-wall contact, local voidage and local gas-solid flow structure can be produced. Such information is essential in determining the heat transfer behavior of individual particles. The approach has been attempted by some investigators to study coal combustion,[19–22] air drying,[23,24] and olefin polymerization.[25] However, in those studies, the heat transfer mode by particle-particle conduction is only partially considered. The analysis of heat transfer mechanisms has not been performed seriously. To date, particle scale study of heat transfer is still not well developed.

In this article, a more comprehensive DPS-CFD approach is proposed to investigate the heat transfer in packed/fluidized beds in connection with the previous attempts. The model is first described in detail. Then, it is tested by comparing the predictions with literature data in terms of effective thermal conductivity (ETC), individual particle HTC, and flow and heat transfer patterns. In particular, the heat transfer characteristics and mechanisms of hot spheres are analyzed quantitatively, and then further examined for different packed/fluidized beds. The extended DPS-CFD model offers a useful numerical technique to elucidate the fundamentals governing the heat transfer in packed/fluidized beds at a particle scale.

Model Description

Governing equations for solid particles

Various methods have been developed for DPS simulation, as reviewed by Zhu et al.[18] In this work, the DPS model is the soft sphere model, i.e., discrete element method (DEM), originally proposed by Cundall and Strack.[26] Thus, a particle in a gas-fluidized bed can have two types of motion: translational and rotational, which are determined by Newton's second law of motion. The governing equations for the translational and rotational motion of particle i with radius R_i, mass m_i, and moment of inertia I_i can be written as

$$m_i \frac{d\mathbf{v}_i}{dt} = \mathbf{F}_{f,i} + \sum_{j=1}^{k_c} \left(\mathbf{F}_{c,ij} + \mathbf{F}_{d,ij}\right) + m_i \mathbf{g} \tag{1}$$

$$I_i \frac{d\boldsymbol{\omega}_i}{dt} = \sum_{j=1}^{k_c} \left(\mathbf{M}_{t,ij} + \mathbf{M}_{r,ij}\right) \tag{2}$$

where $\mathbf{v}_i$ and $\boldsymbol{\omega}_i$ are the translational and angular velocities of the particle, respectively, and k_c is the number of particles in interaction with the particle. The forces involved are: particle-fluid interaction force $\mathbf{F}_{f,i}$, the gravitational force $m_i\mathbf{g}$, and interparticle forces between particles, which include elastic force $\mathbf{F}_{c,ij}$, and viscous damping force $\mathbf{F}_{d,ij}$. These interparticle forces can be resolved into the normal and tangential components at a contact point. The torque acting on particle i by particle j includes two components: $\mathbf{M}_{t,ij}$ which is generated by tangential force and causes particle i to rotate, and $\mathbf{M}_{r,ij}$ commonly known as the rolling friction torque, is generated by asymmetric normal forces and slows down the relative rotation between particles. A particle may undergo multiple interactions, so the individual interaction forces and torques are summed over the k_c particles interacting with particle i. The equations used to calculate the particle-particle interaction forces and torques, and particle-fluid interaction force $\mathbf{F}_{f,i}$ are listed in Table 1. They have been used in our previous studies of particle packing and flow.[27–33]

The heat transfer of particle i and its surroundings is considered to be controlled by three mechanisms: particle-fluid convection, particle-particle or particle-wall conduction, and radiation. According to the energy balance, the governing equation for particle i can be generally written as

$$m_i c_{p,i} \frac{dT_i}{dt} = \sum_{j=1}^{k_i} Q_{i,j} + Q_{i,f} + Q_{i,rad} + Q_{i,wall} \tag{3}$$

where k_i is the number of particles exchanging heat with particle i, $Q_{i,j}$ is the heat exchange rate between particles i and j due to conduction, $Q_{i,f}$ is the heat exchange rate between particle i and its local surrounding fluid, $Q_{i,rad}$ is the heat exchange rate between particle i and its surrounding environment by radiation, and $Q_{i,wall}$ is particle-wall heat exchange rate. $c_{p,i}$ is the particle specific heat at constant pressure. Details for the calculation of each of the heat exchange rates are discussed in the subsection "Heat transfer models".

Governing equations for fluid phase

The continuum fluid field is calculated from the continuity and Navier-Stokes equations based on the local mean variables over a computational cell, which can be written as[27,29]

$$\frac{\partial \varepsilon_f}{\partial t} + \nabla \cdot (\varepsilon_f \mathbf{u}) = 0 \tag{4}$$

Table 1. Components of forces and torque acting on particle i

Forces and torques	Symbols	Equations
Normal elastic force	$\mathbf{F}_{cn,ij}$	$-\frac{4}{3}E^*\sqrt{R^*}\delta_n^{3/2}\mathbf{n}$
Normal damping force	$\mathbf{F}_{dn,ji}$	$-c_n\left(8m_{ij}E^*\sqrt{R^*\delta_n}\right)^{1/2}\mathbf{V}_{n,ij}$
Tangential elastic force	$\mathbf{F}_{ct,ji}$	$-\mu_s\left\|\mathbf{F}_{cn,ij}\right\|(1-(1-\delta_t/\delta_{t,\max})^{3/2})\hat{\delta}_t \quad (\delta_t < \delta_{t,\max})$
Tangential damping force	$\mathbf{F}_{dt,ji}$	$-c_t\left(6\mu_s m_{ij}\left\|\mathbf{F}_{cn,ij}\right\|\sqrt{1-\left\|\mathrm{v}_t\right\|/\delta_{t,\max}}/\delta_{t,\max}\right)^{1/2}\mathbf{V}_{t,ij} \quad (\delta_t<\delta_{t,\max})$
Coulumb friction force	$\mathbf{F}_{t,ji}$	$-\mu_s\left\|\mathbf{F}_{cn,ij}\right\|\hat{\delta}_t \quad (\delta_t \geq \delta_{t,\max})$
Torque by tangential force	$\mathbf{M}_{t,ji}$	$\mathbf{R}_{ij}\times\left(\mathbf{F}_{ct,ij}+\mathbf{F}_{dt,ij}\right)$
Rolling friction torque	$\mathbf{M}_{r,ij}$	$\mu_{r,ij}\left\|\mathbf{F}_{n,ij}\right\|\bar{\omega}_{t,ij}^{n}$
Particle-fluid drag force	$\mathbf{F}_{f,i}$	$0.125C_{d0,i}\rho_f\pi d_i^2\varepsilon_i^2\left\|\mathbf{u}_i-\mathbf{v}_i\right\|(\mathbf{u}_i-\mathbf{v}_i)\varepsilon_i^{-(\chi+1)}$

where $\frac{1}{m_{ij}}=\frac{1}{m_i}+\frac{1}{m_j}$, $\frac{1}{R^*}=\frac{1}{|\mathbf{R}_i|}+\frac{1}{|\mathbf{R}_j|}$, $E^*=\frac{E}{2(1-\nu^2)}$, $\bar{\omega}_{t,ij}=\frac{\omega_{t,ij}}{|\omega_{t,ij}|}$, $\hat{\boldsymbol{\delta}}_t=\frac{\boldsymbol{\delta}_t}{|\boldsymbol{\delta}_t|}$,

$\delta_{t,\max}=\mu_s\frac{2-\nu}{2(1-\nu)}\delta_n$, $\mathbf{V}_{ij}=\mathbf{V}_j-\mathbf{V}_i+\boldsymbol{\omega}_j\times\mathbf{R}_j-\boldsymbol{\omega}_i\times\mathbf{R}_i$, $\mathbf{V}_{n,ij}=(\mathbf{V}_{ij}\cdot\mathbf{n})\cdot\mathbf{n}$, $\mathbf{V}_{t,ij}=(\mathbf{V}_{t,ij}\times\mathbf{n})\times\mathbf{n}$,

$\chi=3.7-0.65\exp[-(1.5-\log_{10}\mathrm{Re}_i)^2/2]$, $C_{d0,i}=(0.63+4.8/\mathrm{Re}_i^{0.5})^2$, $\mathrm{Re}_i=\rho_f d_{pi}\varepsilon_i|\mathbf{u}_i-\mathbf{v}_i|/\mu_f$.

Note that tangential force ($\mathbf{F}_{ct,ij}$+$\mathbf{F}_{dt,ij}$) should be replaced by $\mathbf{F}_{t,ij}$ when $\delta_t \geq \delta_{t,\max}$.

$$\frac{\partial(\rho_f\varepsilon_f\mathbf{u})}{\partial t}+\nabla\cdot(\rho_f\varepsilon_f\mathbf{u}\mathbf{u})=-\nabla p-\mathbf{F}_{fp}+\nabla\cdot\varepsilon_f\tau+\rho_f\varepsilon_f\mathbf{g} \tag{5}$$

By definition, the corresponding equation for heat transfer can be written as

$$\frac{\partial(\rho_f\varepsilon_f c_pT)}{\partial t}+\nabla\cdot(\rho_f\varepsilon_f\mathbf{u}c_pT)=\nabla\cdot(c_p\Gamma\nabla T)+\sum_{i=1}^{k_v}Q_{f,i}+Q_{f,wall} \tag{6}$$

where $\mathbf{u}$, ρ_f, p and $\mathbf{F}_{fp}=(\sum_{i=1}^{k_V}\mathbf{F}_{f,i})/\Delta V$ are the fluid velocity, density, pressure and volumetric fluid-particle interaction force, respectively, and k_V is the number of particles in a computational cell of volume ΔV. Γ is the fluid thermal diffusivity, defined by μ_e/σ_T, and σ_T the turbulence Prandtl number, which is set to 1.0 for this work. $Q_{f,i}$ the heat exchange rate between fluid and particle i which locates in a computational cell, and $Q_{f,wall}$ fluid-wall heat transfer rate. τ and ε_f are the fluid viscous stress tensor and porosity, respectively, which are given as[29]

$$\tau=\mu_e\left[(\nabla\mathbf{u})+(\nabla\mathbf{u})^{-1}\right] \tag{7}$$

$$\varepsilon_f=1-\sum_{i=1}^{k_v}V_i/\Delta V \tag{8}$$

where V_i is the volume of particle i (or part of the volume if the particle is not fully in the cell), μ_e the fluid effective viscosity determined by the standard k-ε turbulent model. Thus, the turbulent kinetic energy and dissipation rate of turbulent kinetic energy are governed by the k-equation

$$\frac{\partial(\rho_f\varepsilon_f k)}{\partial t}+\nabla\cdot(\rho_f\varepsilon_f\mathbf{u}k)=\nabla\cdot\left(\frac{\mu_e}{\sigma_k}\nabla k\right)+G_f-C_D\rho_f\varepsilon_f\varepsilon \tag{9}$$

and the ε-equation

$$\frac{\partial(\rho_f\varepsilon_f\varepsilon)}{\partial t}+\nabla\cdot(\rho_f\varepsilon_f\mathbf{u}\varepsilon)=\nabla\cdot\left(\frac{\mu_e}{\sigma_\varepsilon}\nabla\varepsilon\right)+\frac{\varepsilon}{k}\left(C_1G_f-C_2\rho_f\varepsilon_f\varepsilon\right) \tag{10}$$

where

$$\mu_e(k,\varepsilon)=\mu_f+C_\mu\rho_f\varepsilon_f k^2/\varepsilon \tag{11}$$

$$G_f=\mu_e\left\{2\left[(\partial u_x/\partial x)^2+(\partial u_z/\partial z)^2\right]+(\partial u_x/\partial z+\partial u_z/\partial x)^2\right\} \tag{12}$$

Note that μ_f is the fluid molecular viscosity. The values of other constants used in the above equations are: C_μ= 0.09; C_D = 1.00; C_1 = 1.44; C_2 = 1.92; σ_k = 1.00; σ_ε = 1.30.[34] This k-ε model has been used in our previous study of gas-solid flow.[35]

Heat transfer models

As shown in Eqs. 3 and 6, three heat transfer mechanisms are considered in this DPS-CFD model: fluid-particle or fluid-wall convection; particle-particle or particle-wall conduction; and particle radiation. Different heat transfer models are adopted for these mechanisms, as described in the following.

1. Convective heat transfer

Convective heat transfer between particle and fluid has been extensively investigated since the 1950s, and different

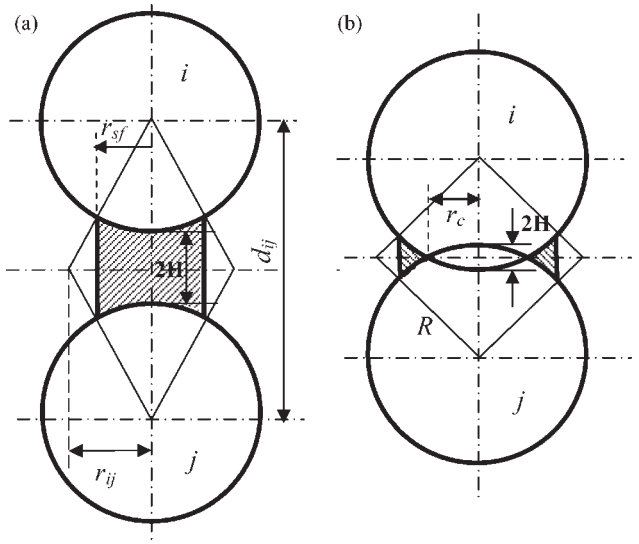

Figure 1. Schematic of the relative positions of two spheres: (a) noncontact, and (b) contact with an overlap.

equations have been proposed.[5–8] Often, the convective heat-transfer rate between particle i and fluid is calculated according to $Q_{i,f} = h_{i,conv} \cdot A_i \cdot (T_{f,i} - T_i)$, where A_i is the particle surface area, $T_{f,i}$ is fluid temperature in a computational cell where particle i is located, and $h_{i,conv}$ is the convective HTC. $h_{i,conv}$ is associated with the Nusselt number, which is a function of particle Reynolds number and gas Prandtl number, given by

$$Nu_i = h_{i,conv} d_{pi}/k_f = 2.0 + a\mathrm{Re}_i^b \mathrm{Pr}^{1/3} \tag{13}$$

where k_f and d_{pi} are the fluid thermal conductivity and particle diameter, respectively. Re_i is the local relative Reynolds number for particle i, and defined in Table 1. The gas (air) Prandtl number Pr, is a material property, and for simplicity, is assumed to be a constant in this work, set to 0.712 corresponding to that for air at 300 K. The constant, 2.0, represents the contribution by particle-fluid natural convection. a and b are two parameters that need to be evaluated. As suggested by Kunii and Levenspiel,[5] b = 0.5, and a could range from 0.6 to 1.8. Based on the recent literature data where the bed conditions are similar to these simulation cases,[13,14,36] the estimated value of a varies slightly around 1.2. Thus, in the present simulation, $a = 1.2$ is adopted.

For fluid-wall heat transfer, $Nu_D = h_{f,wall} D/k_f = 0.023\mathrm{Re}^{0.8}\mathrm{Pr}^n$ is used to determine the heat transfer coefficient $h_{f,wall}$, where D is the hydraulic diameter, and the exponent n is 0.4 for heating, and 0.3 for cooling.[37] Then the heat flux $Q_{f,wall}$ between particle and wall is determined by $Q_{f,wall} = h_{f,wall} \cdot A_{f,wall} \cdot (T_{wall} - T_f)$, where $A_{f,wall}$ is the contact area between fluid and wall.

2. Conductive heat transfer

Conduction between particles involves various mechanisms,[38,39] which mainly include (1) particle-fluid-particle conduction heat transfer; and (2) particle-particle conduction heat transfer, as indicated in Figure 1. The model details for those two mechanisms are described as follows.

Particle-fluid-particle heat transfer has been examined by various investigators.[36,39] In this work, the model proposed by Cheng et al.[39] is used after some modification. According to this model, the heat transfer flux between spheres i and j is written as

$$Q_{i,j} = (T_j - T_i) \times \int_{r_{sij}}^{r_{sf}} \frac{2\pi \cdot r dr}{(\sqrt{R^2 - r^2} - r(R+H)/r_{ij}) \cdot (1/k_{pi} + 1/k_{pj}) + 2[(R+H) - \sqrt{R^2 - r^2}]/k_f} \tag{14a}$$

where

$$H = (d_{ij} - 2R)/2 \tag{14b}$$

$$r_{sf} = \frac{R \cdot r_{ij}}{\sqrt{r_{ij}^2 + (R+H)^2}} \tag{14c}$$

$$r_{ij} = \sqrt{3V_{ij}/(\pi \cdot d_{ij})} \tag{14d}$$

where k_{pi} and k_{pj} are the thermal conductivities of particles i and j, respectively. As shown in Figure 1b, parameter $r_{sij} = 0$ when $H \geq 0$ and $r_{sij} = r_c$ when $H < 0$, where r_c is the radius of the contact area of two contacting particles. r_{ij} is the radius of the lens of fluid between two contacting or near contacting spheres and determined by Eq. 14d. V_{ij} is the volume of Voronoi polyhedra between particles i and j. The structure of fluidized beds varies, and the determination of the transient Voronoi polyhedra for a system composed of a large number of particles is very time-consuming. There is a need to employ a simplified method to overcome this problem. On the other hand, Yang et al.[40] have examined the properties of Voronoi polyhedra for different porosities. The simplification required can be based on their results. Actually there is only one parameter that requires in this heat transfer modeling, i.e., the face area A_{ij} of Voronoi polyhedron between particles i and j. Based on the results of Yang et al.[40] A_{ij} can be written as

$$A_{ij} = \pi \cdot r_{ij}^2 = 0.985 R_i^2 (1 - \varepsilon_i)^{-2/3} \tag{15a}$$

or

$$r_{ij} = 0.560 R_i (1 - \varepsilon_i)^{-1/3} \tag{15b}$$

where ε_i is the local porosity corresponding to particle i, as used in the DPS-CFD calculation. Parameter $2H$, as indicated in Figure 1, is determined by Eq. 14b, where d_{ij} can be obtained from the DPS simulation. Generally, the larger the distance between two non-contacting spheres, the less the heat flux. As shown in Figure 2, the heat flux reduces significantly with the H/R ratio increasing. It can be ignored after a "cut-off" value which is set to 0.5 in the model. The effect of this cut-off value will be further examined in the subsection "Model validation".

Conduction heat transfer always occurs through the contacted area between particles or between particles and wall.

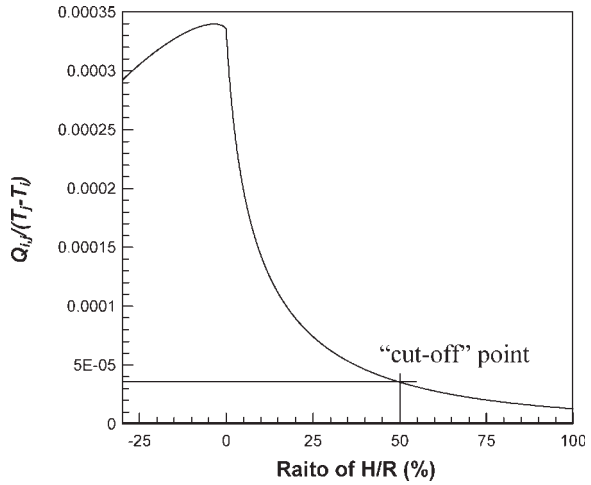

Figure 2. Variation of $Q_{i,j}/(T_j-T_i)$ with the ratio of H/R (%), calculated by Eq. 14a.

Generally, such conduction heat transfer due to elastic deformation includes two mechanisms: conduction due to particle-particle static contact (particularly common in a packed bed), and conduction due to particle-particle collision, which occurs in a moving or fluidized bed.

For conduction due to particle-particle static contact, the equation proposed by Batchelor and O'Brien[41] and modified by Cheng et al.[39] is adopted. Thus, the heat flux $Q_{i,j}$ through the contact area between particles i and j can be calculated according to the following equation

$$Q_{i,j} = \frac{4r_c(T_j - T_i)}{(1/k_{pi} + 1/k_{pj})} \tag{16}$$

Particle-particle heat transfer due to collision is normally determined by the model proposed by Sun and Chen.[42] Recently, Zhou et al.[43] provided a modified equation that can be readily implemented in this DPS-CFD model

$$Q_{i,j} = c' \frac{(T_j - T_i)\pi r_c^2 t_c^{-1/2}}{(\rho_{pi}c_{pi}k_{pi})^{-1/2} + (\rho_{pj}c_{pj}k_{pj})^{-1/2}} \tag{17a}$$

$$c' = 0.435 \cdot \left(\sqrt{c_2^2 - 4c_1(c_3 - F_o)} - c_2\right)/c_1 \tag{17b}$$

$$c_1 = -2.300 \cdot (\rho_{pi}c_{pi}/\rho_{pi}c_{pi})^2 + 8.909 \cdot (\rho_{pj}c_{pj}/\rho_{pj}c_{pj}) - 4.235 \tag{17c}$$

$$c_2 = 8.169 \cdot (\rho_{pi}c_{pi}/\rho_{pi}c_{pi})^2 - 33.770 \cdot (\rho_{pj}c_{pj}/\rho_{pj}c_{pj}) + 24.885 \tag{17d}$$

$$c_3 = -5.758 \cdot (\rho_{pi}c_{pi}/\rho_{pi}c_{pi})^2 + 24.464 \cdot (\rho_{pj}c_{pj}/\rho_{pj}c_{pj}) - 20.511 \tag{17e}$$

$$t_c = 2.94(5m_{ij}/4E_{ij})^{2/5}(R_{ij} \cdot v_{nij})^{-1/5} \tag{17f}$$

where r_c and t_c are particle-particle contact radius and contact duration, respectively. To be consistent with the current model, r_c is obtained from the DEM simulation, which is based on the Hertz elastic contact theory (see Table 1). F_o, the Fourier number, is defined as $\alpha \cdot t_c/(r_c^2)$, where α is particle thermal diffusivity. v_{nij} is the normal relative velocity between particles i and j. For particle-wall static or collision contact, a wall can be treated as a particle with an infinite diameter and mass, as commonly used in the DEM work. Its properties are assumed to be the same as particles in this work.

It should be noted that the two mechanisms represented by Eqs. 16 and 17 must be distinguished in computation. In the simulation, the following method is applied to do so. For fixed beds, particle-particle contacts are all static. Thus, only static contact heat transfer applies. For fluidized beds, two parameters are set: particle-particle collision time t_c, which can be calculated by Eq. 17f, and particle-particle contact duration time t_d, which can be obtained from simulation. For two colliding particles, if $t_c \geq t_d$, only collisional heat transfer applies. If $t_c < t_d$, two particles will keep in touch after collision. In such a case, collision heat transfer applies first during the time of t_c, and then static heat transfer during the time of $(t_d - t_c)$.

3. Radiative heat transfer

In a fixed or fluidized bed, a particle is surrounded by particles and fluid. In a specified enclosed cell, an environmental temperature is assumed to represent the enclosed surface temperature around such a particle. Thus, the equation used by Zhou et al.[21] is slightly modified to calculate the heat flux due to radiation using a local environmental temperature to replace the bed temperature, and is written as

$$Q_{i,rad} = \sigma\varepsilon_{pi}A_i(T_{local,i}^4 - T_i^4) \tag{18}$$

where σ is the Stefan-Boltzmann constant, equal to 5.67×10^{-8} W/(m$^2 \cdot$K^4), and ε_{pi} is the sphere emissivity, set to 0.8 for this work. Gas radiation is not considered in this study due to low-gas emissivities.

The parameter $T_{local,i}$ is the averaged temperature of particles and fluid by volume fraction in an enclosed spherical domain Ω given by

$$T_{local,i} = \varepsilon_f T_{f,\Omega} + (1 - \varepsilon_f)\frac{1}{k_\Omega}\sum_{j=1}^{k_\Omega} T_j (j \neq i) \tag{19}$$

where $T_{f,\Omega}$ and k_Ω are, respectively, the fluid temperature and the number of particles located in the domain Ω. In this work, the domain radius is assumed to be $1.5d_p$. To be fully enclosed, a larger radius can be used.

Heat transfer coefficient

HTC is an important parameter to describe the thermal behavior of particles. For any particle in a particle-fluid system, it involves three basic heat transfer modes, as indicated by Eq. 3. Correspondingly, different HTCs for particle i at time t can be defined in the following

1. Convective HTC between particle and fluid

$$h_{i,conv} = Q_{i,conv}/A_i(T_{f,i} - T_i) \tag{20a}$$

2. Two types of conductive HTCs (''net conductive HTC'' and ''absolute conductive HTC'') are defined, and given by

$$h_{i,cond,net} = \sum_{j=1}^{k_i} h_{ij,cond} + h_{i,wall} = \sum_{j=1}^{k_i} \left[\left|Q_{ij,cond}\right|/A_i(T_j - T_i)\right] + \left|Q_{i,wall}\right|/A_i(T_w - T_i) \quad (20b)$$

$$h_{i,cond,abs} = \sum_{j=1}^{k_i} h_{ij,cond} + h_{i,wall} = \sum_{j=1}^{k_i} \left[\left|Q_{ij,cond}\right|/|A_i(T_j - T_i)|\right] + \left|Q_{i,wall}\right|/|A_i(T_w - T_i)| \quad (20c)$$

where $h_{i,cond,net}$ is the net conductive HTC of particle i between this particle and surroundings, and $h_{i,cond,abs}$ is the absolute conductive HTC. Obviously, under the condition of steady state or thermal equilibrium, $h_{i,cond,net} = 0$.

3. Radiative HTC between particle and environment

$$h_{i,rad} = Q_{i,rad}/A_i(T_{local,i} - T_i) \quad (20d)$$

4. The total HTC for particle i is defined as

$$h_i = (Q_{i,conv} + \sum_{j=1}^{k_i} Q_{ij,cond} + Q_{i,wall} + Q_{i,rad})/A_i(T_b - T_i) \quad (20e)$$

where $Q_{i,conv}$, $Q_{i,cond}$, $Q_{i,wall}$ and $Q_{i,rad}$ in Eq. 20a–e are heat exchange rates between particle i and its surroundings. A_i is the surface area of particle i, and T_b is the bed averaged temperature. Then the transient HTCs ($h_{i,conv}$, $h_{i,cond}$, $h_{i,rad}$ and h_i) for particle i can be calculated by Eqs. 20a–e.

For the cooling of limited individual hot particles in the fluid bed with room temperature condition, the heat always flows from a hot particle to its surroundings, so $h_{i,cond,net} = h_{i,cond,abs}$. Also, it can be assumed that the bed temperature is not affected by the presence of limited hot particles. Under this assumption, $T_j = T_{wall} = T_{f,i} = T_{local,i} = T_b$, and Eq. 20e can be written as

$$h_i = Q_{i,conv}/A_i(T_{f,i} - T_i) + \sum_{j=1}^{k_i} \left[Q_{ij,cond}/A_i(T_j - T_i)\right] + Q_{i,wall}/A_i(T_{wall} - T_i) + Q_{i,rad}/A_i(T_{local,i} - T_i) \quad (20f)$$

or

$$h_i = h_{i,conv} + \sum_{j=1}^{k_i} h_{ij,cond} + h_{i,wall} + h_{i,rad} \quad (20g)$$

It reveals that the total HTC of hot particles is the sum of all sub-HTCs due to different heat transfer mechanisms. This is actually what was used in the so-called hot sphere approach.[13,14] Its validity will be examined later.

HTC varies temporally and spatially. For convenience, the following terms are used in the later discussion: (1) transient HTC of particle i, defined by Eqs. 19 and 20; (2) time-averaged HTC of particle i, defined by $\frac{1}{(t_1-t_0)}\int_{t_0}^{t_1} h_i(t)dt$ where unless otherwise specified, $t_0 = 0$; (3) bed-averaged HTC, defined by $\frac{1}{N}\sum_{i=1}^{N} h_i$, where N is number of particles in a bed, and (4) time-bed-averaged HTC, defined by $\frac{1}{N}\sum_{i=1}^{N}\frac{1}{(t_1-t_0)}\int_{t_0}^{t_1} h_i(t)dt$.

Solutions and coupling schemes

The methods for numerical solution of DPS and CFD have been well established in the literature. For the DPS model, an explicit time integration method is used to solve the translational and rotational motions of discrete particles.[26] For the CFD model, the conventional SIMPLE method is used to solve the governing equations for the fluid phase.[44] The modeling of the solid flow by DPS is at the individual particle level, while the fluid flow by CFD is at the computational cell level. The coupling methodology of the two models at different length scales has been well documented,[27,32,45] and has been successfully used in our previous DPS-CFD studies.[29,31,33,46] This work simply extends that approach to include heat transfer. The coupling scheme used is, therefore, the same. Thus, for each time step, DPS will give information, such as the positions, velocities, and temperatures of individual particles, for the evaluation of porosity, particle-fluid interaction force, and heat flux in a computational cell. CFD will then use these data to determine the gas flow and temperature fields, which then yield the particle-fluid interaction forces acting on individual particles and heat fluxes between fluid and particles. Incorporation of the resulting forces and heat fluxes into DPS will produce information about the motion and temperature of individual particles for the next time step.

Simulation conditions

The geometry used in the present simulation is a two-dimensional (2-D) slot model, as shown in Figure 3a. The model thickness is eight particle diameters. Periodic boundary conditions are applied to the front and rear directions.

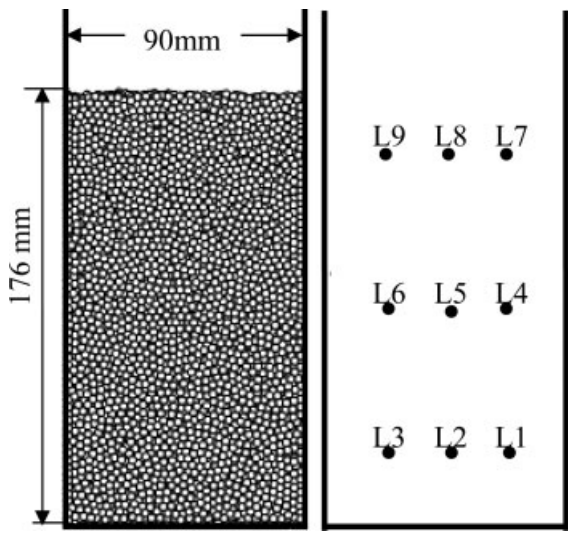

Figure 3. The particle bed used in this study (left), and the initial locations of nine hot bronze spheres (right).

Table 2. Parameters used in the present simulations

Variables	Values
Bed width	90 mm
Bed thickness	24 mm
Bed height	176 mm
Total CFD cells	15×150
Cell size ($\Delta x \times \Delta z$)	6 mm×6 mm
Number of particles (N)	16,000
Diameter of bed particles (d_p)	3 mm
Diameter of hot spheres (d_p)	3 mm
Density of bed particles (ρ_p)	420 kg/m^3
Density of hot spheres (ρ_p)	8,850 kg/m^3
Thermal conductivity of bed particles (k_p)	0.84 W/(m·K)
Thermal conductivity of hot spheres (k_p)	55 W/(M·k)
Specific heat capacity of bed particles (c_p)	800 J/(kg·K)
Specific heat capacity of hot spheres (c_p)	351 J/(kg·K)
Initial temperature of bed particles	25°C
Initial temperature of hot spheres	180°C
Particle-particle/wall sliding friction (μ_s)	0.4
Particle-particle/wall rolling friction (μ_r)	1%d_p mm
Particle-particle/wall damping (c_n=c_t)	0.3
Particle Young's modulus (E)	5.0×10^9 kg/(m·s^2)
Particle poisson ratio (v)	0.3
Time step (Δt)	1.75×10^{-7} s
Type of fluid	Air
Fluid temperature (T_f)	25°C, 100°C, 1000°C
Fluid density (ρ_f)	By state equation*
Fluid molecular viscosity (μ_f)	By Sutherland's formula**
Fluid thermal conductivity (k_f)	$2.873\times10^{-2}+7.76\times10^{-5}\times(T_f+273)$ W/(m·K)
Fluid specific heat capacity (c_{pf})	$1002.737+1.2324\times10^{-2}\times(T_f+273)$ J/(kg·K)
Fluid Prandtl number (Pr)	0.712
Fluid superficial velocity (U)	0.1∼1.8 m/s

*State of equation: $\rho = PM/(RT_f)$ where P=101325 Pa, M=0.029 kg/mol, R=8.314 J/(mol K)
**Sutherland formula[47] is written as: $\mu_f = C_1T^{3/2}/(T+C_2)$ where $C_1 = 1.511 \times 10^{-6}$ Kg/(m·s·K$^{1/2}$), C_2=120K.

For such a geometry, 2-D CFD and 3-D DPS are employed in this work as used elsewhere.[31,33] The bed used is packed with particles of 3 mm diameter, and then fluidized by uniform gas introduced from the bed bottom. The bed minimum fluidization velocity U_{mf} is 0.6 m/s at room temperature condition, determined from simulation. It should be noted that, unless otherwise specified, the thermal conductivity of bed particles is k_p= 0.84 W/(m·K). Table 2 lists the parameters used in the simulation. The simulations are conducted mainly under the following two conditions for different purposes:

1. Hot sphere simulation at room temperature (25°C for gas and bed particles, 180°C for hot spheres). This condition allows to examine the cooling behavior of limited hot spheres immersed in a bed. For the purpose of comparison with the literature measurements, the properties of hot spheres used are the same as those in the experiment of Collier et al.[13] During the cooling of a bronze sphere, its thermal parameters such as temperature and transient HTCs can be readily obtained. Also, the effect of initial locations of hot spheres is examined. As shown in Figure 3b, each location (L1∼L9) corresponds to a hot sphere, although much of our discussion is based on the bronze sphere initially located at L8. Moreover, the effect of thermal conductivity is also examined.

2. Bed heating process by hot gas: This condition allows the examination of the thermal behavior of all particles in a bed. The bed is initially at room temperature of 25°C, then heated by hot gas (100 or 1,000°C) which is introduced uniformly from the bottom. During the heating, the thermal behavior of all particles is examined and analyzed.

Results and Discussion

Model validation

In the following discussion the validity of the proposed approach is examined from three different aspects.

1. Flow patterns in gas fluidization

Gas fluidization is an operation by which solid particles are transformed into a fluid-like state through suspension in a gas.[5] Different flow patterns can be generated by varying gas velocity, which can be reproduced by this DPS-CFD approach. As shown in Figure 4, at a low-gas superficial velocity ($U = 0.33U_{mf}$ where U_{mf} = 0.6 m/s), particles in the bed remain stationary, and gas passes through the voids among particles. This state is identified as a fixed or packed bed ($U < U_{mf}$). When the interaction force between particles and gas just counterbalances the total weight of particles, the bed starts fluidization, and the gas velocity at this point is referred to as the minimum fluidization velocity (U_{mf}). With further increase in U ($>U_{mf}$), the gas-solid flow behaves

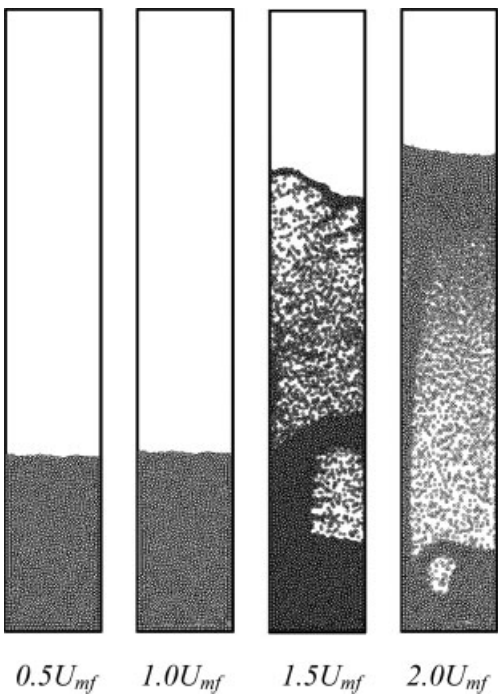

Figure 4. Snapshots of solid-flow patterns at different gas superficial velocities when t = 2.0 s.

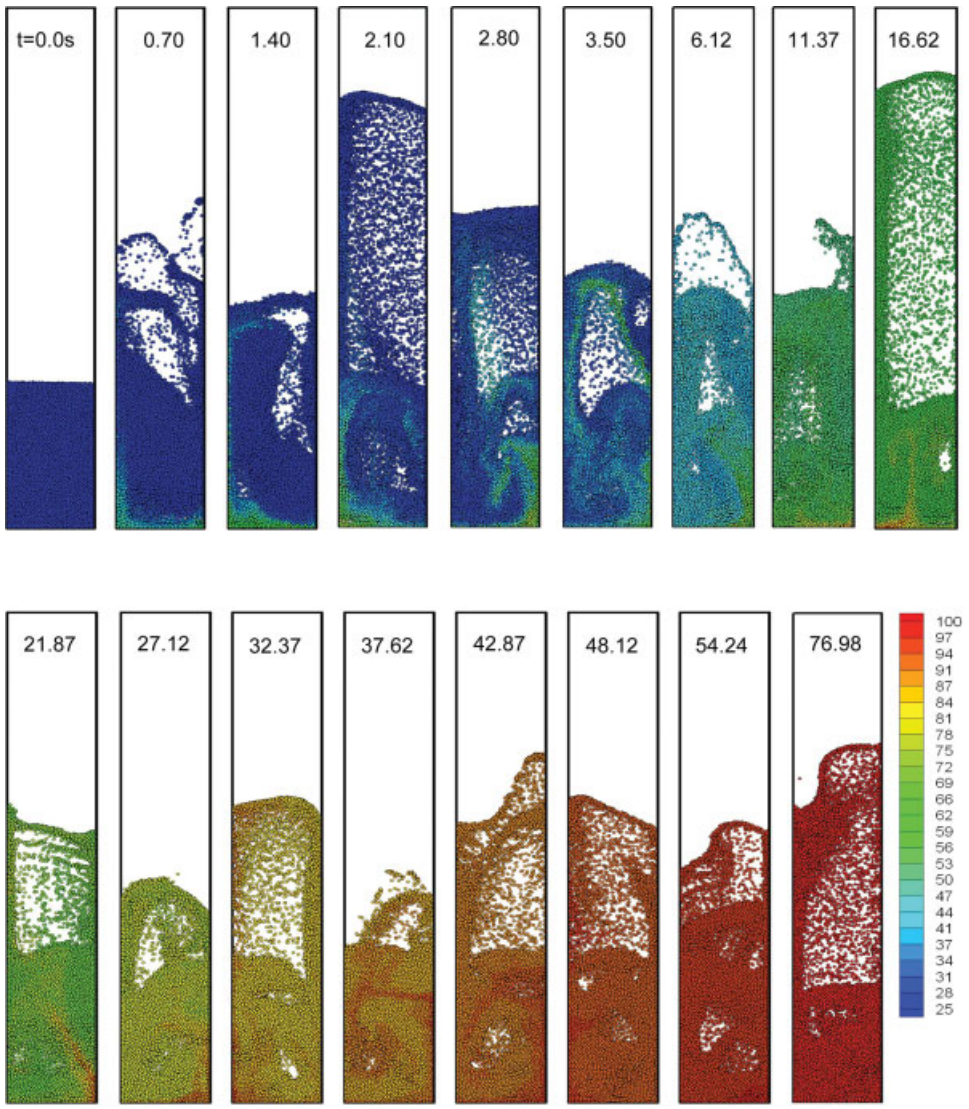

Figure 5. Snapshots showing the heating process of fluidized bed by hot gas (1.2 m/s, 100°C) uniformly introduced from the bottom where the particle temperature (°C) is colored (bed initial temperature: 25°C; and the wall temperature assumed to be 25°C during the simulation). [Color figure can be viewed in the online issue, which is available at www.interscience.wiley.com.]

quite differently, with gas bubbles formed and particles moving in the bed rigorously.

Conditions of gas fluidization determine different flow and heat transfer behavior of particles. The solid flow patterns in gas fluidization are transient and vary with time, as shown in Figure 5 when gas superficial velocity is 1.2 m/s. The figure also illustrates the variation of particle temperature. It can be observed that particles located at the bottom are heated first, and flow upward dragged by gas. Particles with low temperatures descend and fill the space left by those hot particles. Due to the strong mixing and high gas-particle heat transfer rate, the whole bed is heated quickly, and reaches the gas inlet temperature around 70 s. The heating rate is large at early stage due to large temperature difference between gas and particles and between cold and hot particles. Then it slows down gradually because of the decreased temperature difference between gas and particles, as shown in Figure 6. The result in the figure also indicates that it may need a long time to obtain the thermal equilibrium between gas and solid phases.

The general features observed are qualitatively in good agreement with those reported in the literature, confirming the predictability of the proposed DPS-CFD model in dealing with the gas-solid flow and heat transfer in gas fluidization. This will be further confirmed in the discussion of other results.

2. Effective thermal conductivity in a packed bed with stagnant fluid

ETC is an important parameter to measure the thermal efficiency of a packed bed, and has been examined extensively in the past.[48–50] For the purpose of validation, DPS is used to predict the bed ETC based on the proposed model. The method for determining the ETC is similar to the one of Cheng et al.[39] A packed bed is generated first by DPS, then the temperatures at the bed bottom and top are set to constants, $T_{bot} = 125°C$ and $T_{top} = 25°C$, respectively. Then a uniform heat flux q is

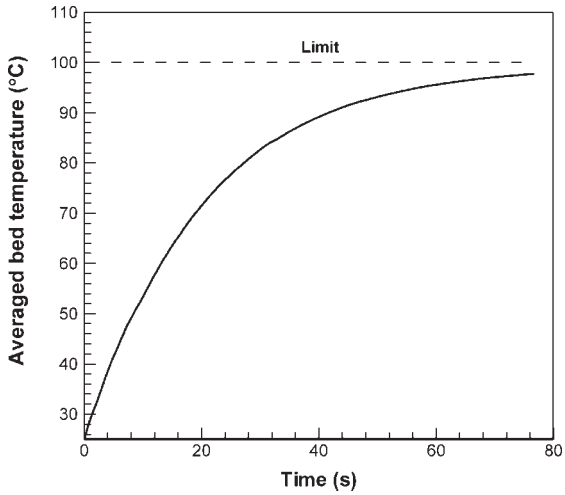

Figure 6. Average bed temperature with time when U/U_{mf} = 2.0.

generated and passes from the bottom to the top. The side faces are assumed to be adiabatic to produce an unidirectional heat flux. The bed ETC is calculated by $k_e = q \cdot H_b(T_{bot} - T_{top})$, where H_b is the height of the bed considered. In this calculation of the bed ETC, only the particle-particle conduction is considered. The convection by the stagnant fluid and the radiation are ignored, because the corresponding heat fluxes are relatively small under the conditions considered.

Figure 7 shows the calculated bed ETC against the ratios of particle thermal conductivity and fluid thermal conductivity. It can be observed that, when Young's modulus E is 5 GPa, the predicted ETCs are comparable with the experimental results when the ratio of thermal conductivities k_p/k_f is low, but slightly overestimated for higher k_p/k_f ratios. With a higher Young's modulus E, i.e., 50 GPa, the predicted and measured ETCs match each other better, as seen in Figure 7. The use of a small Young's modulus in DEM can significantly reduce the computational cost, but leads to a large particle-particle overlap and contacting area. For high particle thermal conductivities, the influence of such an enlarged contact area on the bed ETC becomes more significant, and the ETC is overestimated. However, for most of the cases considered in this work, the ratio of thermal conductivities of bed particles to fluid is small (logarithmic value is 1.46 when k_p = 0.84 W/(m·K)), and the heat flux between particles is controlled by the particle with smaller thermal conductivity. According to Figure 7, the use of a slightly lower Young's modulus will not affect the calculated thermal properties when the logarithmic value of the ratio is less than 2.0.

The predicted ETC is also affected by the ratio of H/R, as mentioned earlier. As shown in Figure 7, the curves are almost the same if H/R is greater than 0.5, confirming that for the system considered, heat transfer between two spheres can be ignored when the particle-particle gap 2H is greater than particle radius R.

3. Cooling of hot spheres

The validity of the proposed model is further examined by considering the cooling of a hot sphere in a fluidized bed. In physical experiments, the temperature of hot spheres is measured directly using thermocouples connected to the spheres.[13,14] In this DPS-CFD simulation, the cooling process of such hot spheres can be easily traced and recorded. As shown in Figure 8, the predicted temperature is comparable with the measured one. At the time around 30 s, the spheres traced are cooled down to room temperature. The cooling curves of nine hot spheres (L1 ~ L9) are slightly different, indicating that the thermal behavior of hot spheres varies with their initial locations. More detailed analysis of the hot sphere approach is given in the following.

Analysis of thermal behavior of hot spheres

HTC is mainly used to analyze the thermal behavior of particles. Here, the thermal characteristics of hot spheres are

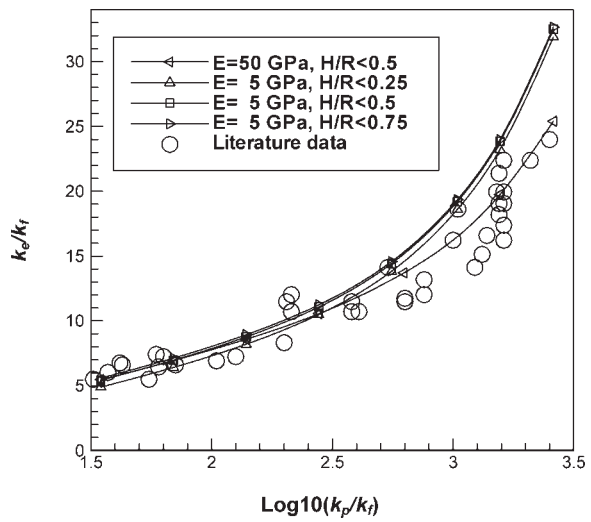

Figure 7. The relationship between effective thermal conductivity and the particle thermal conductivity in a packed bed with stagnant fluid.

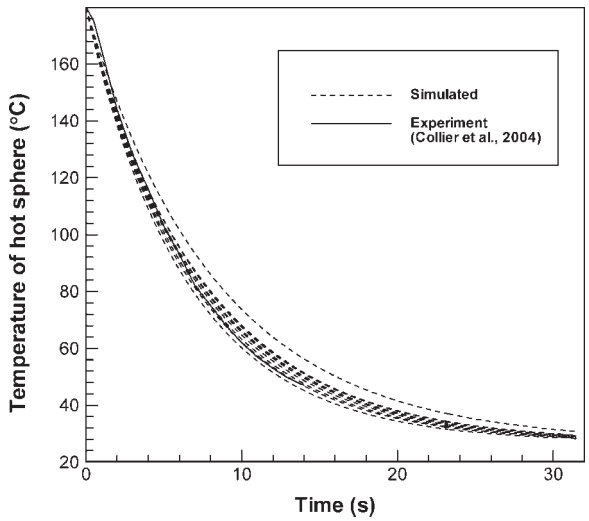

Figure 8. Temperature evolution of hot spheres (diameter of 2 mm) when gas superficial velocity is 0.42 m/s (nine lines are for the nine hot spheres at different initial locations).

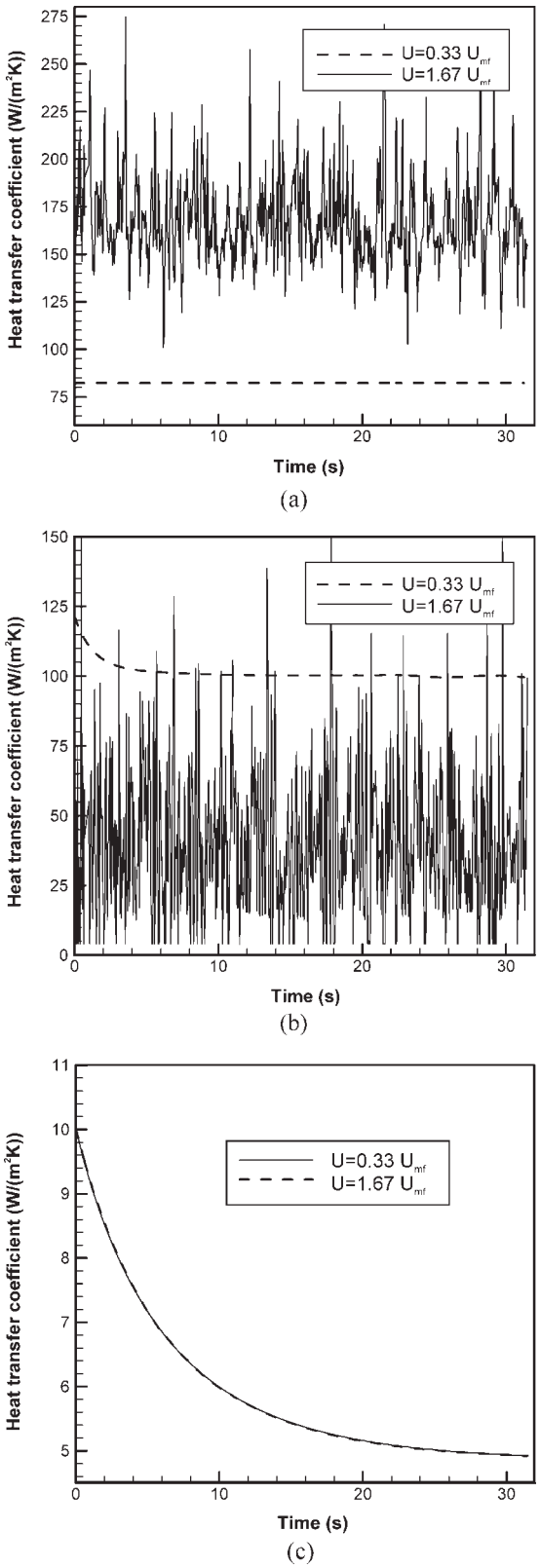

Figure 9. Variation of heat-transfer coefficients of a hot sphere (L8) with time due to: (a) fluid convection; (b) particle conduction, and (c) radiation, calculated according to Eq. 20a, b and 20d, respectively.

presented first to illustrate the advantages of the proposed DPS-CFD model and its predictability in dealing with heat transfer on a particle scale. As an example, Figure 9a and b show the variation of transient HTCs for sphere L8 with time for different gas superficial velocities. It can be observed that both transient convective and conductive HTCs are constants in the fixed bed ($U = 0.33\ U_{mf}$), but fluctuate around a certain value in the fluidized bed ($U = 1.67\ U_{mf}$). This is because, in the fixed bed, the local fluid flow field and packing structure around the hot sphere are stable, and do not change with time. However, in the fluidized bed, the bed flow pattern varies temporally (Figure 5). The movement of a hot sphere is macroscopically chaotic, depending on the forces acting on it. The local structure, and, hence, fluid flow surrounding the hot sphere vary, which causes the fluctuated HTCs.

It is noted that the transient radiative HTC defined by Eq. 20d varies with time, decreasing from 10 $W/(m^2 \cdot K)$ at the initial state to 5 $W/(m^2 \cdot K)$ at the final state (Figure 9c). Compared with the contributions by convection and conduction, radiation contribution is quite small at a low temperature (180°C for hot spheres).

The local fluid flow and particle structure for each sphere (L1–L9) are different. Thus, the time-averaged HTC varies with particle locations, as shown in Figure 10. In the fixed bed, such a variation is mainly contributed by the difference in the local structures surrounding the hot sphere. However, in the fluidized bed, it is mainly contributed by the transient local structure and particle-particle contacts or collisions. Those factors determine the variation of the time-averaged HTCs of hot spheres in a fluidized bed.

Experimentally, Collier et al.[13] and Scott et al.[14] used different materials to examine the HTCs of hot spheres, and found that there is a general tendency that the HTC of hot sphere increases first with gas-superficial velocity in the fixed bed ($U < U_{mf}$), and then remains constant, independent of the gas superficial velocities for fluidized

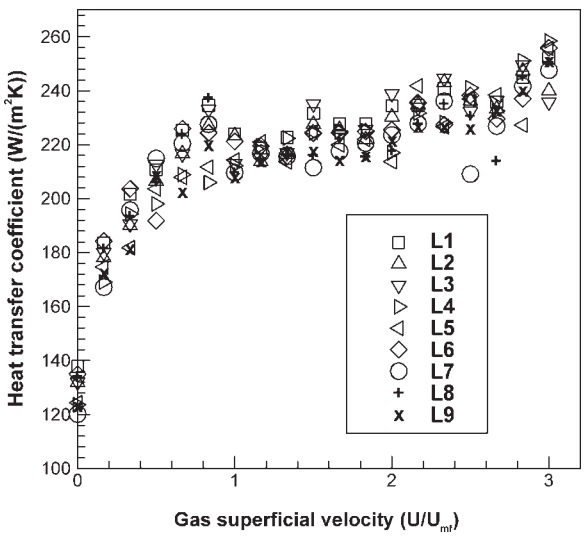

Figure 10. Time-averaged heat transfer coefficients, calculated according to Eq. 20e, of the nine hot spheres as a function of gas superficial velocity.

beds ($U > U_{mf}$). The present simulation results also exhibit such a feature, as shown in Figure 10. For packed beds, the time-averaged HTC increases with gas-superficial velocity, and reaches its maximum around $U = U_{mf}$. After the bed is fluidized, the HTC is almost constant in a large range. However, it should be noted that, with further increasing gas superficial velocity, the particles in the bed can be entrained by gas. The HTC may increase slightly due to the increased dominance of fluid convection and decreased conduction contribution, for example, when $U = 3.0\ U_{mf}$.

However, the general relationship between HTC and gas superficial velocity U as reported by Collier et al.[13] and Scott et al.[14] is not always valid. In fact, the relationship is affected by particle and fluid properties, i.e., the thermal conductivity in particular. To highlight this effect, Figure 11a shows the HTC-U relationships for different particle thermal conductivities k_p, while the thermal conductivity of hot sphere keeps unchanged. It can be observed that the higher the k_p, the higher the HTC of hot spheres. For $k_p = 30$ W/(m·K), the predicted HTC in the fixed bed ($U/U_{mf} < 1$) is so high that the trend of HTC-U relationship shown in Figure 10 is totally changed. For high k_p, the HTC decreases with U in the fixed bed, then may reach a constant HTC in the fluidized bed. However, for a very low thermal conductivity of particles, i.e., $k_p = 0.08$ W/(m·K) shown in Figure 11a, the HTC always increases with U, independent of bed state.

It should be noted that the dashed line in Figure 11a represents the total HTC, which is the sum of different sub-HTCs (Eqs. 20f–g). Although slightly higher than the total HTC, defined by Eqs. 20e, such a difference can be ignored. It confirms that, for the cooling case of hot spheres, the particle total HTC can be roughly treated as the sum of all sub-HTCs. Thus, it will enable us to further analyze those sub-HTCs as in the following.

The mechanisms controlling the HTC-U relationship can be identified by the current proposed model, and shown in Figure 11b. As indicated in Eq. 20, the HTC for the hot sphere mainly consists of three mechanisms: convective HTC between particle and fluid, conductive HTC between particles, and radiative HTC. For the case considered, the radiative HTC is very small (Figure 9c), and ignored in Figure 11b together with the particle-wall HTC. From Figure 11b, it can be seen that the convective HTC increases with gas superficial velocity, not sensitive to particle thermal conductivity. However, particle thermal conductivity affects the conductive HTC significantly, particularly in the fixed bed. It indicates that, for high particle thermal conductivities, particle-particle conduction through the contact area is important in fixed beds. However, such a sensitivity of conductive HTC on k_p is significantly reduced in fluidized beds because of the reduced particle-particle contacts. Thus, the effect of k_p on the HTC-U relationship shown in Figure 11a is mainly determined by the conductive HTC.

Figure 11b indicates that, generally, the convective HTC increases with U; but conductive HTC decreases with U. For a proper particle thermal conductivity, i.e., 0.84 W/(m·K), the two contributions (convective HTC and conductive HTC) could compensate each other, then the total HTC is nearly constant after the bed is fluidized. So HTC independence of U is valid under this condition, which is consistent with that

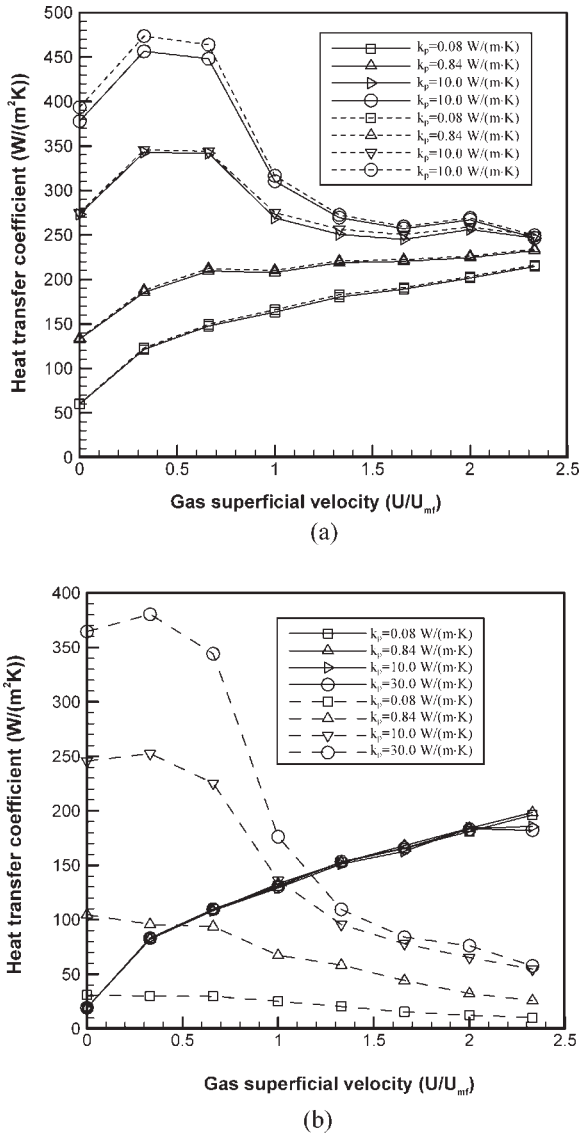

Figure 11. Time-averaged heat transfer coefficients of: (a) total (solid line, calculated by Eq. 20e; dash line, calculated by Eq. 20f), and (b) convection (solid line, calculated by Eq. 20a), and conduction (dashed line, calculated by Eq. 20b), respectively, for hot sphere L8 for different particle thermal conductivities.

reported by Collier et al.[13] and Scott et al.[14] However, if particle thermal conductivity is too low or too high, the relationship of HTC and U can be different, as revealed in Figure 11a.

The proposed DPS-CFD model has also been used to analyze the submechanisms in conduction. As indicated in Figure 1, three mechanisms are considered in conduction: particle-fluid-particle for two non-contacting particles (Figure 1a), particle-fluid-particle for two contacting particles (Figure 1b), and particle-particle through the contacting area in Figure 1b. The relative contributions by these heat transfer paths can be quantified, and shown in Figure 12. Here, the

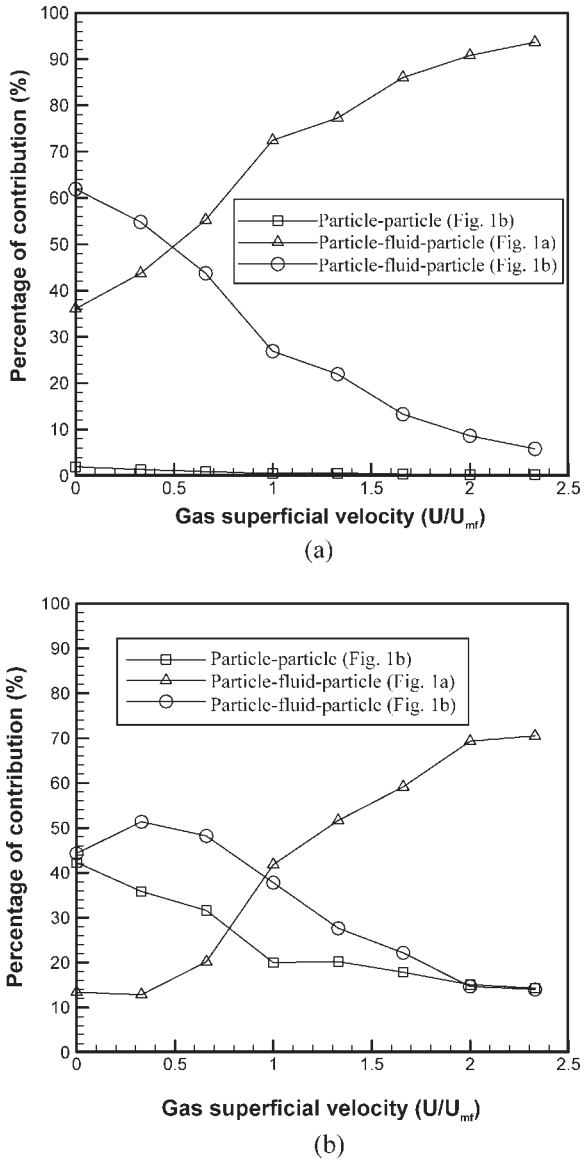

Figure 12. Contributions to conduction heat transfer by different heat transfer mechanisms under the condition of (a) k_p = 0.08 W/(m · K), and (b) k_p = 30 W/(m · K).

relative contribution by each conduction mode is illustrated by the percentage which is defined as the ratio of heat transferred by each conduction mode to the total conduction heat when the hot sphere cools from initial temperature 180 to 30°C. As shown in Figure 12a, under the condition of k_p = 0.08 W/(m · K), particle-fluid-particle conduction always contributes more than particle-particle contact for the case considered (e.g., small thermal conductivity of bed particles), but both vary with gas superficial velocity. For particle-fluid-particle conduction, particle-fluid-particle heat transfer with two contacting particles is far more important than that with two non-contacting particles in the fixed bed. This is because the hot sphere contacts about six particles when $U < U_{mf}$. However, such a feature changes in the fluidized bed ($U > U_{mf}$), where particle-fluid-particle conduction between non-contacting particles is relatively more important. This is because most of particle-particle contacts with an overlap are destroyed gradually with increasing gas superficial velocity, which significantly reduces the contribution by particle-fluid-particle between two contacting particles.

Particle-particle conduction through the contacting area becomes more important with an increase of particle thermal conductivity. As indicated in Figure 12b, the percentage of its contribution is up to 42% in the fixed bed when k_p = 30 W/(m·K), then reduces to around 15% in the fluidized bed. Correspondingly, the contribution percentage by particle-fluid-particle heat transfer is lower, but the trend of variation with gas superficial velocity is similar to that for k_p = 0.08 W/(m·K). Note that the contribution by collision (Eq. 17a–f) is very small, only around 0.5%, and is, thus, ignored in this discussion. The numerical result confirms the literature understanding, which, although, is not so quantitative.[19,22,24,25]

Heat transfer characteristics of a packed/fluidized bed

A particle-fluid bed has many particles. The analysis of the heat transfer of hot spheres is indeed at an individual particle scale. However, a limited number hot spheres cannot represent fully the averaged thermal behavior of all particles in a bed. Thus, there is a need to examine the HTCs of all the particles, and find out the particle thermal characteristics statistically. In this section, the averaged thermal properties, mainly the HTC, of all the particles in a packed/fluidized bed are examined and analyzed. The case used is based on the bed heating process as indicated in the simulation conditions and Figure 5. As mentioned earlier, for this analysis, we use the concepts such as bed-averaged, time-averaged, and time-bed-averaged HTCs. It should be noted that the conductive HTC includes "net conductive HTC" and "absolute conductive HTC". Thus, the bed-averaged net conductive HTC defined by Eq. 20b should be zero (conduction through wall ignored here), although the conduction heat transfer contributes to the realization of bed thermal equilibrium. Unless otherwise specified, therefore, the conductive HTC discussed below is based on Eq. 20c.

Figure 13 shows the bed-averaged sub-HTCs (convective HTC in Figure 13a, and conductive HTC in 13b) over the whole bed as a function of time for different gas superficial velocities. The features shown are similar to those observed in Figure 9a and b for hot spheres. Such a similarity illustrates that the hot sphere approach can, at least partially, represent the general features of particle thermal behavior in a particle-fluid bed. From Figures 13, it can be observed that the bed-averaged sub-HTCs are constant in the fixed bed (e.g., $U = 0.67U_{mf}$). When $U \geq U_{mf}$, HTCs fluctuate around a certain value with time. With the increase of gas superficial velocity, the convective HTC increases (Figure 13a), but conductive HTC decreases (Figure 13b). The relationship of sub-HTCs and gas-superficial velocities can be further revealed in Figure 14. The HTC due to fluid convection increases with gas superficial velocity, but HTC due to particle conduction decreases. Under the low temperature conditions, the radiative HTC is very small.

Overall, the particles in a uniformly fluidized bed behave similarly. However, a particle may behave differently from one another at a given time. Figure 15a shows the

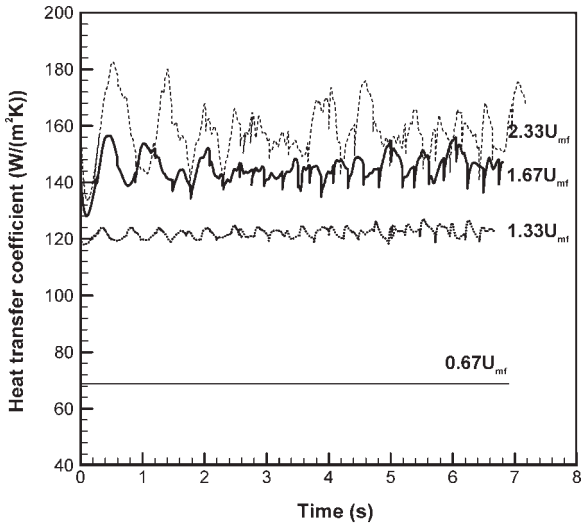

(a)

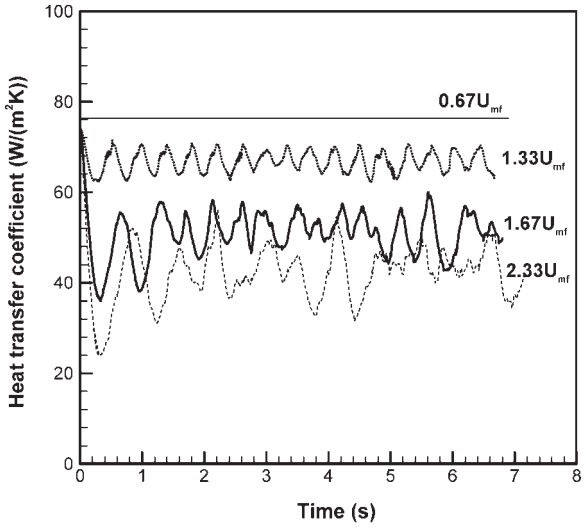

(b)

Figure 13. Bed-averaged heat-transfer coefficients as a function of time for different gas superficial velocities; (a) particle-fluid convection, and (b) particle conduction, calculated according to Eq. 20a and c, respectively.

probability density distributions of time-averaged HTCs due to particle-fluid convection. It can be seen that the convective HTC in the packed bed varies in a small range due to the stable particle structure. Then the distribution curve moves to the right as gas superficial velocity increases, indicating the increase of convective HTC. The distribution curve also becomes wider. This is because, in a fluidized bed, clusters and bubbles can be formed, and the local flow structures surrounding particles vary in a large range.

The density distribution of time-averaged HTCs by conduction is shown in Figure 15b. In the packed bed, it has a wider distribution (curves 1, 2 and 3), indicating different local packing structures for particles. However, curves 1 and 2 are similar. This is because, statistically, the two bed packing structures are similar, and do not vary much even if gas superficial velocity is different. When $U > U_{mf}$ (e.g., $U = 2.0\ U_{mf}$), the distribution curve moves to the left, indicating the heat transfer due to interparticle conduction is reduced. The bed particles occasionally collide and contact each other. Statistically, the number of collisions and contacts are similar in fully fluidized beds, and not affected significantly by gas superficial velocities. Those features are consistent with those observed using the hot sphere approach, i.e., the HTC variation with locations (Figure 10), and the conductive HTC variation with gas superficial velocities (Figure 11b). It confirms that hot sphere approach can represent the thermal behavior of all bed particles to some degree.

The particle thermal behavior in the fluidized bed is affected by many factors, including (1) gas superficial velocity, (2) particle thermal conductivity, and (3) bed temperature. The effects of gas superficial velocity and particle thermal conductivity have been discussed earlier. The effect of bed temperature is demonstrated in the following example.

It has been shown that the contribution by radiation is small for low bed operation temperature (100°C), as seen in Figure 14. However, if the bed operating temperature is greater than 500°C, the radiation will contribute significantly to the overall heat transfer.[17] To highlight the effect of bed operating temperature, Figure 16 shows the variation of the bed-averaged HTCs with time due to different heat transfer mechanisms for the case of gas superficial velocity 3.2 m/s, and its temperature 1,000°C under the fluidized condition. It can be seen that the radiative HTC increases with time due to the increase of the bed temperature. At a high temperature, e.g., 900°C, the radiative HTC reaches 300 $W/(m^2 \cdot K)$, which is significantly larger than that for the case of hot gas with 100°C (ca. 5 $W/(m^2 \cdot K)$ as indicated in Figure 14. Due to the variation of gas properties with temperature, i.e., the thermal conductivity, density and specific heat (shown in

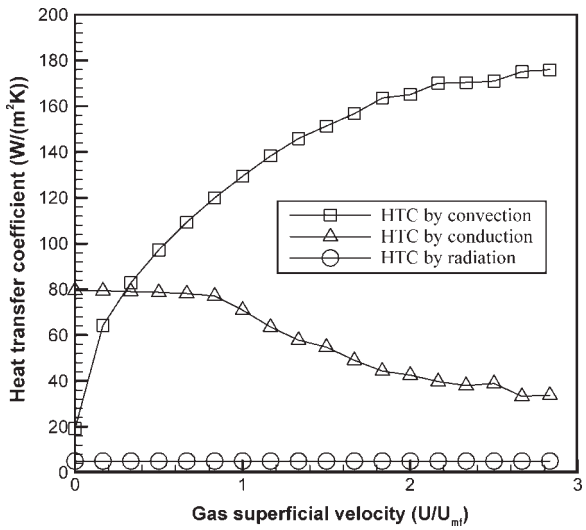

Figure 14. Bed-averaged convective, conductive and radiative heat transfer coefficients (calculated according to Eq. 20a, c and d, respectively) as a function of gas superficial velocity.

Table 2), the convective and radiative HTCs do not remain constant during the bed heating. However, the conductive heat transfer coefficient is not affected much by the bed temperature. This is because the conductive HTC is quite small in the fluidized bed, and only related to the gas and particle thermal conductivities.

It should be noted that this analysis of heat transfer characteristics was made mainly in terms of HTC. According to Eqs. (20a–c), the convective HTC ($h_{i,conv}$) and conductive HTC ($h_{ij,cond}$) are independent of particle temperature after combining with the heat flux correlations $Q_{i,conv}$, $Q_{ij,cond}$ and $Q_{i,wall}$, respectively, although their magnitudes depend on the local fluid flow and particle structure. However, this consideration is not applicable to the radiation HTC. This is because radiative HTC can be obtained by combining Eqs. 18 and 20d, giving $h_{i,rad} = \sigma\varepsilon_{pi}(T_{local,i} + T_i)(T_{local,i}^2 + T_i^2)$. It is temperature-dependent, increasing with the bed temperature, as shown in Figure 16. Such results do not fully describe the heat transfer features, which also highlights the limitation of HTC in heat transfer analysis.

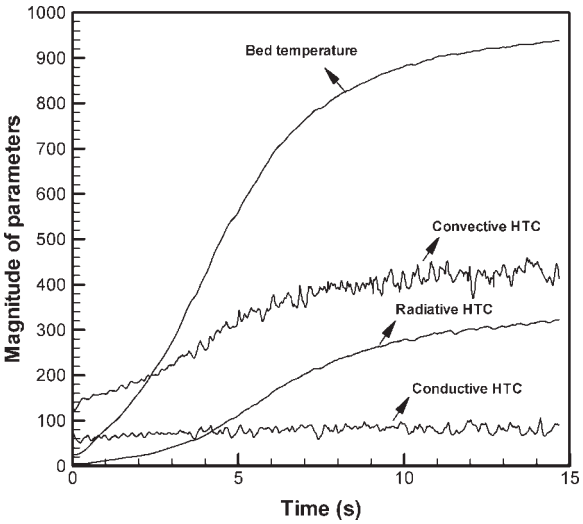

Figure 16. Thermal behavior of bed particles under the condition of gas inlet temperature 1,000°C, and superficial velocity 3.2 m/s.

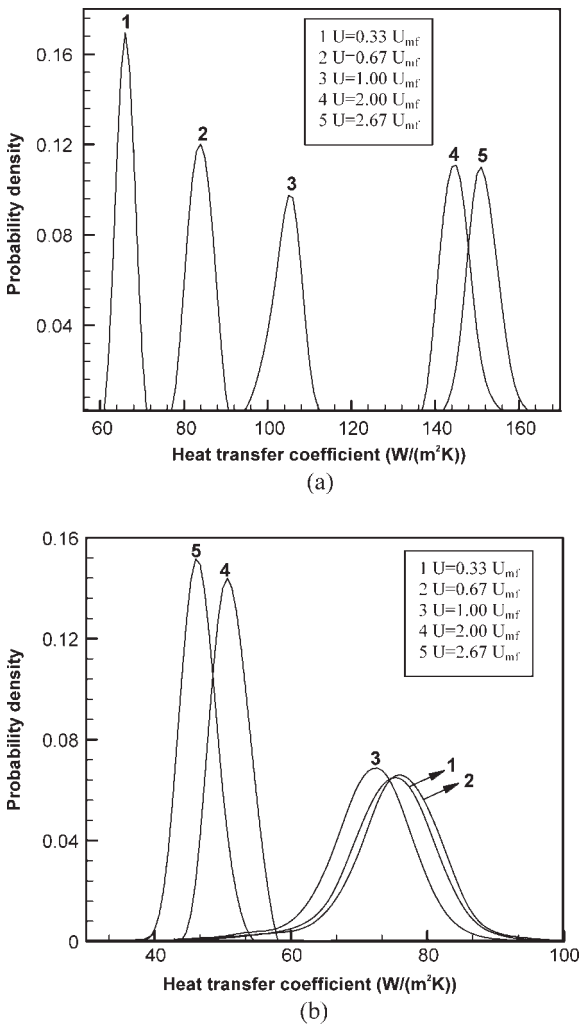

Figure 15. Probability density distributions of time-averaged heat transfer coefficients of particles at different gas superficial velocities; (a) fluid convection, and (b), particle conduction, calculated according to Eq. 20a and c, respectively.

Limitation of the proposed approach

Heat transfer in packed and fluidized beds involves phenomena at different time and length scales. For example, with reference to particles, heat flow can occur within a particle at a subparticle scale, between particles at a particle scale, and between clusters of particles and between particles and fluid at a local average (meso) scale, in addition to the overall heat transfer at a macro, process equipment scale. Corresponding to the discrete particle simulation, this approach can generate information to understand the heat transfer in a fluid bed at a particle scale, which is very useful for better fundamental understanding of the role of various heat transfer mechanisms as demonstrated earlier. However, at this stage of development, it has some limitations as discussed below.

In mathematical form, Eq. 3 is the same as the so-called lumped-capacity formulation, where the thermal resistance within a particle can be neglected.[37] This condition is reasonable when the Biot number, defined as $h \cdot (V_p/A_p)/k_p$, is less than 0.1. However, as noted earlier, in this approach, Eq. 3 is established on the basis of energy balance at a particle scale. So, the parameters (e.g., m, c_p, T, and k_p) involved should be the representative properties of the considered particle at this scale. So is the case for the equations used to calculate the heat fluxes involved. In general, such information should be obtained from the studies at a subparticle scale. Indeed, some of the equations employed in this work are generated from such subparticle scale studies; see, for example, Eqs. 14, 16 and 17 for conductive heat transfer, some of which were determined from the finite element method (FEM). However, some are just based on the correlations available in the literature, e.g., Eq. 13 for convective heat transfer; in addition to the simplification introduced in the calculation of radiative heat transfer (see Eqs. 18 and

19). Many of these equations were not originally formulated for particle scale studies. Moreover, the limitations associated with these equations will be inherited in this approach. For example, it is not clear if Eq. 13 is applicable to particle mixtures, and the local temperature in Eq. 18 is affected by the domain size.

To overcome the problems identified above, intensive and long-term studies, particularly at a subparticle scale, are needed. This consideration applies to the particle scale study of granular flow, as noted by Zhu et al.[18] In fact, even limited to particle-fluid flow, investigators are now still struggling to generate a more accurate equation to calculate the particle-fluid drag force, involving the use of advanced numerical technique such as Lattice Boltzmann method.[51,52] On the other hand, since particle scale modeling is almost a first principle approach, the inaccuracy at a subparticle scale may not affect the accuracy at particle and larger scales much. This consideration has been well received in granular dynamics simulation.[53] It may also apply to the heat transfer studies. Indeed, the results shown in this work demonstrate the proposed approach is very promising in elucidating the heat transfer mechanisms in packed/fluidized beds. It also offers a general model framework for further developments in the future.

Conclusions

The DPS-CFD approach, originally applied to study the particle-fluid flow, has been extended in this work to study the heat transfer in packed and bubbling fluidized beds at a particle scale. The proposed model is, either qualitatively or quantitatively depending on the observations in the literature, validated by comparing the predicted and measured results under different conditions. Three basic heat transfer modes (particle-fluid convection, particle conduction and radiation) are considered in this model, and their contributions to the total heat transfer in a fixed or fluidized bed can be quantified and analyzed. This is important to better understanding and controlling the heat transfer in fluid-bed reactors.

The examination of thermal behavior of hot spheres indicates that, in a fixed bed, the particle HTC remains constant with time, but varies slightly with locations. With the increase of gas superficial velocity U, the HTC increases. In a fluidized bed, the particle HTC fluctuates around a certain value with time. The magnitude of the HTC is determined by the local flow structure. However, the time-averaged HTC is independent of U. Those features are consistent with literature findings.[13,14] The independency of HTC on U can be explained by the balanced compensation of the increase of convective heat transfer between gas and particles, and the decrease of conductive heat transfer between particles. However, such a relationship is significantly affected by particle thermal conductivity k_p and bed temperature. For high k_p, the conduction is dominant in the fixed bed due to the large heat flux through the particle-particle contact area, showing the decrease of the time-averaged HTC with U increasing. For low k_p, the HTC-U relationship is featured by the gradual increase of HTC with U, independent of bed state. The examination of the effect of bed temperature reveals that the particle HTC increases with time. This is because of the increased contribution of radiation with the increase of bed temperature during the bed heating process. The results confirm that at high temperatures, radiation plays an important role in the overall particle heat transfer.

The hot sphere approach as illustrated in the current simulation is able to represent the features of bed thermal behavior to some degree, e.g., the temporal and spatial HTC variation of a sphere considered with time and space, and the averaged HTC-U relationship. However, it may have a difficulty to generate reliable and accurate data about sub-HTCs, and their statistical distributions corresponding to different heat transfer mechanisms. The results also show that the proposed DPS-CFD model offers an effective method to overcome this problem, which is important for a better understanding of the coupled fluid flow and heat transfer in packed and fluidized beds. However, there is a need for further studies to generalize the approach.

Acknowledgements

The authors are grateful to the Australian Research Council and BlueScope Steel Research for the financial support of this work.

Notation

A_i = surface area of particle i, m^2
A_{ij} = face area of Voronoi polyhedron between particles i and j, m^2
C_{d0} = fluid drag coefficient on an isolated particle, dimensionless
c_n = normal damping coefficient, dimensionless
c_t = tangential damping coefficient, dimensionless
c_p = particle specific heat capacity, J/(kg·K)
c_{pf} = fluid specific heat, J/(kg·K)
d_{ij} = distance between the centers of particle i and j, m
d_p = particle diameter, m
E = Young's modulus, Pa
$\boldsymbol{F}_c$ = particle-particle contact force, N
$\boldsymbol{F}_d$ = particle-particle damping force, N
$\boldsymbol{F}_{fp}$ = volumetric fluid-particle interaction force, N/m^3
$\boldsymbol{F}_{f,i}$ = particle-fluid interaction force on particle i, N
Fo = Fourier number, dimensionless
$\boldsymbol{g}$ = gravitational acceleration, m/s^2
G_f = defined by Eq. 12, $kg/(m \cdot s^3)$
H = defined by Eq. 14b, m
H_b = height between two layers with two constant temperatures, m
h = heat transfer coefficient, $W/(m^2 \cdot K)$
$\boldsymbol{I}$ = moment of inertia of particle, $kg \cdot m^2$
k = turbulence kinetic energy, m^2/s^2
k_c = number of particles in contact with particle i, dimensionless
k_e = effective thermal conductivity, W/(m·K)
k_f = fluid thermal conductivity, W/(m·K)
k_i = number of particles in interaction (including heat transfer) with particle i, dimensionless
k_p = particle thermal conductivity, W/(m·K)
k_v = number of particles in a computational cell, dimensionless
k_Ω = Number of particles located in a domain Ω, dimensionless
$\boldsymbol{M}_r$ = rolling torque, N·m
$\boldsymbol{M}_t$ = tangential torque, N·m
m = mass of particle, kg
N = number of particles in a bed, dimensionless
Nu = Nusselt number, dimensionless
Q = heat exchange rate, W
q = heat exchange rate per unit of area, W/m^2
p = fluid pressure, Pa
Pr = Prandtl number, dimensionless
$\boldsymbol{R}$ = vector from the mass center of the particle to the contact point, m
R = particle radius, m
r_c = particle-particle contact radius, m
r_{ij} = defined by Eq. 14d, m
r_{sf} = defined by Eq. 14c, m

r_{sij} = radius of the contact circle between particles i and j, m
Re = Reynolds number, dimensionless
T = temperature, K
T_b = bed temperature, K
t = time, s
t_c = time of particle-particle collision, s
t_d = time of particle-particle contact, s
$\boldsymbol{u}$ = fluid velocity, m/s
U = gas superficial velocity, m/s
U_{mf} = Minimum fluidization velocity, m/s
$\boldsymbol{v}$ = particle translational velocity, m/s
$v_{n,ij}$ = normal relative velocity between particles i and j, m/s
V = volume of particle, m^3
V_{ij} = volume of Voronoi polyhedra between particles i and j, m^3
ΔV = volume of a computational cell, m^3
x=x = direction in a coordinate system, m
Δx = width of a computational cell, m
x=z = direction in a coordinate system, m
Δz = height of a computation cell, m

Greek letters

Γ = fluid thermal diffusivity, m^2/s
α = particle thermal diffusivity, m^2/s
χ = empirical coefficient defined in Table 1, dimensionless
$\delta_{t,max}$ = maximum δ_t when sliding starts, m
$\boldsymbol{\delta}_n$ = relative normal displacement at contact, m
$\boldsymbol{\delta}_t$ = relative tangential displacement at contact, m
$\hat{\boldsymbol{\delta}}_t$ = unit vector of δ_t, dimensionless
ε_f = porosity, dimensionless
ε_i = porosity, dimensionless
ε_{pi} = particle emissivity, dimensionless
ε = dissipation rate of turbulent kinetic energy, m^2/s^3
μ_f = fluid molecular viscosity, kg/(m·s)
μ_e = fluid effective viscosity, kg/(m·s)
μ_r = rolling friction coefficient, m
μ_s = sliding friction coefficient, dimensionless
ν = poisson ratio, dimensionless
ρ = density, kg/m^3
σ = Stefan-Boltzmann constant, $W/(m^2 \cdot K^4)$
σ_T = Turbulence Prandtl number, dimensionless
τ = stress tensor, Pa
$\boldsymbol{\omega}$ = angular velocity, 1/s
$\hat{\boldsymbol{\omega}}$ = unit vector of ω, dimensionless

Subscripts

c = contact
d = damping
f = fluid
i = particle i
ij = between particles i and j
j = particle j
n = Normal component
p = particle
r = rolling
t = tangential component
w = wall

Abbreviation

abs = absolute
$cond$ = conduction
$conv$ = convection
ETC = effective thermal conductivity
HTC = heat transfer coefficient
rad = radiation

Literature Cited

1. Omori Y. *Blast Furnace Phenomena and Modeling*. London: Elsevier Applied Science; 1987.
2. Dong XF, Yu AB, Yagi JI, Zulli P. Modelling of multiphase flow in a blast furnace: Recent developments and future work. *ISIJ Int*. 2007;47:1553–1570.
3. Avedesian MM, Davidson JF. Combustion of carbon particles in a fluidized bed. *Trans Inst Chem Eng*. 1973;51:121–131.
4. Oka SN. *Fluidized Bed Combustion*. New York: Marcel Dekker, Inc.; 2004.
5. Kunii D, Levenspiel O. *Fluidization Engineering*. Boston: Butterworth-Heinemann; 1991.
6. Botterill JSM. *Fluid-bed heat transfer*. New York: Academic Press; 1975.
7. Wakao N, Kaguei S. *Heat and mass transfer in packed beds*. New York: Gordon and Breach; 1982.
8. Molerus O, Wirth KE. *Heat transfer in fluidized beds*. London: Chapman and Hall; 1997.
9. Prins W, Draijer W, van Swaaij WPM. *Heat transfer to immersed spheres fixed or freely moving in gas-fluidized bed*. In: Van Swaaij WPM, Afgan NH. *Heat and Mass Transfer in Fixed and Fluidized Beds*. New York: Hemisphere; 1986:317–331.
10. Baskakov AP, Filippovskii N, Munts VA, Ashikhmin AA. Temperature of particles heated in a fluidized bed of inert material. *J Eng Phys*. 1987;52:788–793.
11. Agarwal PK. Transport phenomena in multi-particle systems-IV. Heat transfer to a large freely moving particle in gas fluidized bed of smaller particles. *Chem Eng Sci*. 1991;46:1115–1127.
12. Parmar MS, Hayhurst AN. The heat transfer coefficient for a freely moving sphere in a bubbling fluidized bed. *Chem Eng Sci*. 2002;57:3485–3494.
13. Collier AP, Hayhurst AN, Richardson JL, Scott SA. The heat transfer coefficient between a particle and a bed (packed or fluidized) of much larger particles. *Chem Eng Sci*. 2004;59:4613–4620.
14. Scott SA, Davidson JF, Dennis JS, Hayhurst AN. Heat transfer to a single sphere immersed in beds of particles supplied by gas at rates above and below minimum fluidization. *Ind Eng Chem Res*. 2004;43:5632–5644.
15. Mickley HS, Fairbanks DF. Mechanism of heat transfer to fluidized beds. *AIChE J*. 1955;1:374–385.
16. Chen JC. Surface contact - Its significance for multiphase heat transfer: Diverse examples. *J Heat Transfer - Trans ASME*. 2003;125:549–566.
17. Chen JC, Grace JR, Golriz MR. Heat transfer in fluidized beds: design methods. *Powder Technol*. 2005;150:123–132.
18. Zhu HP, Zhou ZY, Yang RY, Yu AB. Discrete particle simulation of particulate systems: theoretical developments. *Chem Eng Sci*. 2007;62:3378–3396.
19. Rong DG, Horio M. DEM simulation of char combustion in a fluidized bed. Second International Conference on CFD in the Minerals and Process Industries, Melbourne, Australia; 1999:65–70.
20. Peters B. Measurements and application of a discrete particle model (DPM) to simulate combustion of a packed bed of individual fuel particles. *Combust Flame*. 2002;131:132–146.
21. Zhou HS, Flamant G, Gauthier D, Flitris Y. Simulation of coal combustion in a bubbling fluidized bed by distinct element method. *Chem Eng Res Design*. 2003;81:1144–1149.
22. Zhou HS, Flamant G, Gauthier D. DEM-LES simulation of coal combustion in a bubbling fluidized bed: Part II: coal combustion at the particle level. *Chem Eng Sci*. 2004;59:4205–4215.
23. Li JT, Mason DJ. A computational investigation of transient heat transfer in pneumatic transport of granular particles. *Powder Technology*. 2000;112:273–282.
24. Li JT, Mason DJ. Application of the discrete element modeling in air drying of particulate solids. *Drying Technol*. 2002;20:255–282.
25. Kaneko Y, Shiojima T, Horio M. DEM simulation of fluidized beds for gas-phase olefin polymerization. *Chem Eng Sci*. 1999;54:5809–5821.
26. Cundall PA, Strack ODL. A discrete numerical model for granular assemblies. *Geotechnique*. 1979;29:47–65.
27. Xu BH, Yu AB. Numerical simulation of the gas-solid flow in a fluidized bed by combining discrete particle method with computational fluid dynamics. *Chem Eng Sci*. 1997;52:2785–2809.
28. Zhou YC, Wright BD, Yang RY, Xu BH, Yu AB. Rolling friction in the dynamic simulation of sandpile formation. *Physica A*. 1999;269:536–553.
29. Xu BH, Yu AB, Chew SJ, Zulli P. Numerical simulation of the gas-solid flow in a bed with lateral gas blasting. *Powder Technol*. 2000;109:13–26.

30. Yu AB. Discrete element method - an effective method for particle scale research of particulate matter. *Eng Comput*. 2004;21:205–214.
31. Feng YQ, Xu BH, Zhang SJ, Yu AB, Zulli P. Discrete particle simulation of gas fluidization of particle mixtures. *AIChE J*. 2004;50: 1713–1728.
32. Feng YQ, Yu AB. Assessment of model formulations in the discrete particle simulation of gas-solid flow. *Ind Eng Chem Res*. 2004;43: 8378–8390.
33. Feng YQ, Yu AB. Microdynamic modeling and analysis of the mixing and segregation of binary mixtures of particles in gas fluidization. *Chem Eng Sci*. 2007;62:256–268.
34. Launder BE, Spalding DB. The numerical computation of turbulent flows. *Comput Methods Appl Mech Eng*. 1974;3:269–289.
35. Zhang SJ, Yu AB, Zulli P, Wright B, Tüzün U. Modelling of the solids flow in a blast furnace. *ISIJ Int*. 1998;38:1311–1319.
36. Delvosalle C, Vanderschuren J. Gas-to-particle and particle-to-particle heat-transfer in fluidized-beds of large particles. *Chem Eng Sci*. 1985;40:769–779.
37. Holman JP. *Heat Transfer*. 5th ed. New York: McGraw-Hill Company; 1981.
38. Yagi S, Kunii D. Studies on effective thermal conductivities in packed beds. *AIChE J*. 1957;3:373–381.
39. Cheng GJ, Yu AB, Zulli P. Evaluation of effective thermal conductivity from the structure of packed bed. *Chem Eng Sci*. 1999;54: 4199–4209.
40. Yang RY, Zou RP, Yu AB. Voronoi tessellation of the packing of fine uniform spheres. *Phys Rev E*. 2002;65:041302.
41. Batchelor GB, O'Brien RW. Thermal or electrical conduction through a granular material. *Proceedings of the Royal Society of London Series A-Mathematical and Physical Sciences*. 1997;355: 313–333.
42. Sun J, Chen MM. A theoretical analysis of heat transfer to particle impact. *Int J Heat Mass Transfer*. 1988;31:969–975.
43. Zhou JH, Yu AB, Horio M. Finite element modeling of the transient heat conduction between colliding particles. *Chem Eng J*. 2007; 139:510–516.
44. Patankar SV. *Numerical heat transfer and fluid flow*. New York: Hemisphere, 1980.
45. Xu BH, Feng YQ, Yu AB, Chew SJ, Zulli P. A numerical and experimental study of gas-solid flow in a fluid-bed reactor. *Powder Handling Process*. 2001;13:71–76.
46. Yu AB, Xu BH. Particle-scale modelling of gas-solid flow in fluidization. *Journal of Chemical Technology and Biotechnology*. 2003; 78:111–121.
47. Crane Corporation. *Flow of fluids through valves, fittings, and pipe*. 1988: Technical paper No. 410, published by Crane Company.
48. Kunii D, Smith JM. Heat transfer characteristics of porous rocks. *AIChE J*. 1960;6:71–78.
49. Bauer R, Schlunder EU. Effective radial thermal conductivity of packing in gas flow, part I: thermal conductivity of the packing fraction without gas flow. *Int Chem Eng*. 1978;18:189–204.
50. Tsotsas E, Schlunder EU. Impact of particle size dispersity on thermal conductivity of packed beds: measurement, numerical simulation, prediction. *Chem Eng Technol*. 1991;14:421–427.
51. Hill RJ, Koch DL, Ladd AJC. Moderate-Reynolds-number flows in ordered and random arrays of spheres. *J Fluid Mech*. 2001;448: 243–278.
52. Sankaranarayanan K, Shan X, Kevrekidis IG, Sundaresan S. Analysis of drag and virtual mass forces in bubbly suspensions using an implicit formulations of the Lattice Boltzmann method. *J Fluid Mech*. 2002;452:61–96.
53. Zhu HP, Zhou ZY, Yang RY, Yu AB. Discrete particle simulation of particulate systems: A review of major applications and findings. *Chem Eng Sci*. 2008;63:5728–5770.

Manuscript received Nov. 22, 2007, revision received Sept. 5, 2008, and final revision received Jan. 2, 2009.